DOI: 10.1002/ejic.201100319

$Mg_{1-y}Sc_yZn_2$: Limited Sc/Mg Alloying between Laves Phase $MgZn_2$ and $ScZn_2$ – What Drives $ScZn_2$ into a High-Pressure Phase?

Wenliang Wang,[a] Guihuan Chen,[a] Yixiu Wang,[a] and Qisheng Lin*[a]

Dedicated to Professor John D. Corbett on the occasion of his 85th birthday

Keywords: Intermetallic phases / Solid-state reactions / Laves phases / Solid-state structures / Bonding

A series of solid solutions between the $MgZn_2$ and $ScZn_2$ isostructural Laves phases at 400 °C was synthesized by fusion of stoichiometric metals by conventional solid-state high-temperature means. X-ray diffraction analyses revealed that the alloys remain in space group $P6_3/mmc$, with a = 5.228–5.249 Å and c = 8.532–8.487 Å. The lattice parameters of the solid solution exhibit anisotropic variations: a increases and c decreases with increased starting Sc content (x) in $Mg_{1-x}Sc_xZn_2$. The anisotropic changes correspond to the variations of bond lengths in the ab plane and the interlayer bonds in c. Under the applied reaction conditions, the maximum Sc content was estimated to be $y_{max} \approx 0.47$–0.50 in the formula of $Mg_{1-y}Sc_yZn_2$. Theoretical calculations on a hypothetical $ScZn_2$ model extrapolated for normal pressure revealed that it had higher density-of-states (DOS) and evident Zn–Zn antibonding states at the Fermi energy, meaning that high pressure is necessary to counteract the internal stress resulting from antibonding states.

Introduction

In recent years, polar intermetallics have attracted extensive attention in the field of solid-state chemistry.[1–7] Broadly speaking, polar intermetallics are electronically positioned between the classical Zintl phase and the electron (or Hume-Rothery) phases.[8] In polar intermetallics,[1,7] active metals do not always simply contribute all of their valence electrons to the anionic clusters or networks as those in Zintl phases; instead, they could exhibit some covalent bonding with more electronegative components. Therefore, electron counting rules suitable for Zintl phases[9–11] and for electron phases[12,13] do not apply for polar intermetallics. In terms of electronic structure,[7] polar intermetallics keep their metallic characters; however, low density-of-states or pseudogaps are always found around the Fermi energy as a result of strong covalent bonding within the anionic frameworks.

The AB_2 Laves phases,[14] represented by the cubic $MgCu_2$ or C15 (in *Strukturbericht* designation)[15] phase, the hexagonal $MgZn_2$ (or C14),[16] and the $MgNi_2$ (or C36) phase,[17] are a special class of polar intermetallics that contain interweaving diamond-like network of electropositive A atoms and the network of electronegative B atoms. Laves phases can also be regarded as tetrahedrally close-packed structures, in which each A atom is enclosed by a Frank–Kasper polyhedron[18] (16 vertices decorated with 12 B atoms and 4 A atoms) and each B atom surrounded by an icosahedron formed by 6 A atoms and 6 B atoms. For this reason, Laves phases have been considered as important relatives to icosahedral quasicrystals,[19] which are typical Hume-Rothery phases.[12] The stability of Laves phases has been mainly considered in view of two major concepts: the geometrical[20–22] and electronic rules.[23] The geometric rule, based on close packing of different sized atoms, generalizes that Laves phases form under the condition r_A/r_B = 1.15–1.30, with an ideal value of 1.225. The electronic factor of the stability of Laves phases has been discussed in terms of valence electron concentration (VEC), electronegativity, and chemical bonding, and so on. Nevertheless, all these rules are of low predictability and cannot be used ubiquitously, as critically assessed by Stein and coworkers.[24] For example, the average VEC for $ScZn_2$ is 2.33, this value lies at the boundary between the $MgZn_2$-type (1.80–2.32) and the $MgCu_2$-type Laves phase (>2.32 or <1.80).[24] More recently, various bonding features of Laves phases have also been investigated by using modern ELI-D analyses that suggest an important role of charge transfer from different components.[25]

According to earlier experience, $MgZn_2$-type Laves phases are often accounted as byproducts in tuning Sc–Mg–Zn quasicrystals from $Mg_{2-x}Sc_xZn_{11}$ (x = 0–1) reactions,[26] and the shifts of diffraction peaks in powder X-ray patterns

[a] Department of Chemistry, University of Science and Technology of China,
Hefei, Anhui 230026, P. R. China
E-mail: linqs@ustc.edu.cn

Supporting information for this article is available on the WWW under http://dx.doi.org/10.1002/ejic.201100319.

are found to be dependent on x. These suggest that various Sc/Mg mixtures exist in the corresponding Laves-type phase. However, there are no systematic studies on the structure and bonding of the $Mg_{1-x}Sc_xZn_2$ phase. Since both $MgZn_2$ and $ScZn_2$ Laves phases are isostructural, one could infer that they can easily form a solid solution in the whole composition range. But the $ScZn_2$ Laves phase was reported to be a high-pressure phase only,[27] and the ambient pressure modification of $ScZn_2$ was reported to adopt the AlB_2-type structure;[28] therefore, the solid solution between $MgZn_2$ and $ScZn_2$ is probably not as simple as imagined. This work tries to obtain detailed experimental results on the $Mg_{1-x}Sc_xZn_2$ solid solution and to afford theoretical analyses to elucidate the driving force for the high-pressure $ScZn_2$ phase.

Results and Discussion

Phase Width

Powder X-ray diffraction data show that all reactions of $Mg_{1-x}Sc_xZn_2$ (x = 0–1) yielded approximately 70–80 vol.-% of the desired Laves phase (Figure S1). The peak positions of the target Laves phases shift as a function of x, as expected, suggesting different Sc/Mg mixtures in the structure. According to the refined lattice parameters, shown in Figure 1 and Table S1, the variations for a and c are different: a gradually increases as x increases, whereas c decreases as x increases. As a result, the unit cell volume decreases in the range x = 0–0.33 but increases in the range x = 0.33–0.75 (Table S1). For this reason, single crystals from products of x = 0.25 and 0.50, belonging to the two ranges, were selected as representatives to determine the refined Sc composition y in the formula $Mg_{1-y}Sc_yZn_2$ (Table 1).

Because of the presence other Sc-containing impurity phases in the products, for example, $Sc_{13}Zn_{58}$ and Sc–Mg–Zn icosahedral quasicrystals (cf. Figure S1), the refined y values in $Mg_{1-y}Sc_yZn_2$ are not surprisingly smaller than the corresponding x values (Table 1). Although the maximum value of y (y_{max}) in $Mg_{1-y}Sc_yZn_2$ was not determined experimentally, a value of $y_{max} \approx 0.42$–0.50 could be extrapolated (Figure 1) for a reaction of $x \rightarrow 1$, by assuming that the $ScZn_2$ phase exists at normal pressure and that the $MgZn_2$–$ScZn_2$ system follows the empirical Vegard's law in the whole composition range. The extrapolation suggests that the $MgZn_2$–$ScZn_2$ solid solution has a limited composition range under the current reaction conditions. It also suggests that a reaction with a starting composition ratio of Sc/Zn = 1:2 can not yield the pure $ScZn_2$ Laves phase under normal pressure, which is consistent with the fact that the phase is only synthetically available under high-pressure conditions. On the other hand, supposing that the $ScZn_2$ Laves phase is stable at the normal pressure,[27] its lattice parameters would be estimated to be $a \approx 5.295$ Å and $c \approx 8.302$ Å (Figure 1), yielding a unit cell volume of $V \approx 202.14$ Å^3. The last value is not only smaller than that of the $ScZn_2$ Laves phase at high pressure (202.42 Å^3),[27] but also smaller than that of $MgZn_2$ (202.37 Å^3),[29] an obviously impossible situation when the metallic radii of Mg and Sc (1.598 vs. 1.620 Å for CN = 12)[30] are considered. The force that drives the $ScZn_2$ Laves phase to a high-pressure phase will be discussed below from the viewpoint of structure and bonding.

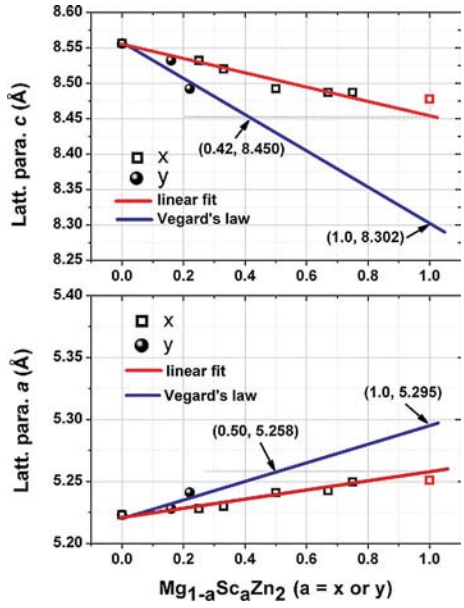

Figure 1. The relationship between the experimental lattice parameters a and c as a function of the starting composition x and the refined composition y in $Mg_{1-a}Sc_aZn_2$ (a = x or y). Red squares denote experimental values of $ScZn_2$ obtained at high pressure.

Table 1. Atomic coordinates and equivalent isotropic displacement parameters for $Mg_{0.84(1)}Sc_{0.16(1)}Zn_2$ and $Mg_{0.78(1)}Sc_{0.22(1)}Zn_2$.[a] U_{iso} is defined as one third of the trace of the orthogonalized $\mathbf{U}_{ij}$ tensor.

	Wyck.	Symm.	Occ.	x	y	z	U_{iso} (Å^2)
Zn1	2*a*	–3*m*.	1	0 0	0 0	0 0	0.013(1) 0.014(1)
Zn2	6*h*	*mm*2	1	0.8301(1) 0.8298(1)	0.6602(1) 0.6596(2)	1/4 1/4	0.013(1) 0.014(1)
Sc/Mg3	4*f*	3*m*.	0.84/0.16(1) 0.78/0.22(1)	1/3 1/3	2/3 2/3	0.0622(2) 0.0618(5)	0.012(1) 0.012(2)

[a] The data for $Mg_{0.84(1)}$ $Sc_{0.16(1)}Zn_2$ comes first.

Structure

Figure 2 shows the crystal structure of the $Mg_{1-y}Sc_yZn_2$ phase. Crystal data and structure refinement for $Mg_{0.84(1)}Sc_{0.16(1)}Zn_2$ and $Mg_{0.78(1)}Sc_{0.22(1)}Zn_2$ are given in Table 2. The structure features a three-dimensional framework of face-shared $(Zn1)_3(Zn2)_9$ Friauf polyhedra (shaded), in which the electropositive Sc/Mg mixtures are hosted. A Friauf polyhedron is a truncated tetrahedron, containing four hexagonal and four triangular faces. In this polyhedron, the three vertices of the waist are exclusively occupied by Zn1 atoms, and the remaining vertices are occupied by Zn2. The Sc–Zn1 and Sc–Zn2 distances are slightly different, approximately 3.03 and 3.07 Å, respectively. The Sc atoms form a hexagonal diamond network, with interatomic separations of about 3.2 Å. Within the anionic framework, Zn1 and Zn2 play distinguished roles. The Zn2 atoms form typical 3636 Kagomé nets at z = 1/4 and 3/4. Note that there are two sets of triangles in the Kagomé nets: one set with shorter edges of approximately 2.56 Å, and another set with longer edges of approximately 2.66 Å. The Zn1 atoms cap the triangles with longer edges from above and below, but leave the smaller triangles empty to interact with Sc/Mg atoms in the Friauf polyhedra.

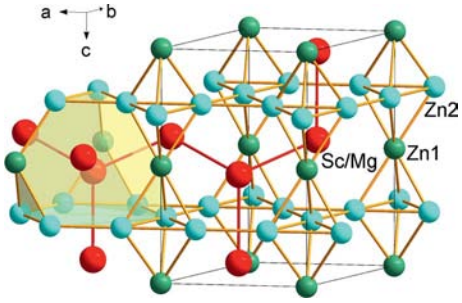

Figure 2. Crystal structure for $Mg_{1-y}Sc_yZn_2$. Each Sc is enclosed by a Friauf polyhedron (as shaded) defined by three Zn1 and nine Zn2 atoms.

Table 2. Crystal data and structure refinement for $Mg_{0.84(1)}Sc_{0.16(1)}Zn_2$ and $Mg_{0.78(1)}Sc_{0.22(1)}Zn_2$.

Formula	$Mg_{0.84(1)}Sc_{0.16(1)}Zn_2$	$Mg_{0.78(1)}Sc_{0.22(1)}Zn_2$
Formula weight	158.30	159.54
Space group	$P6_3/mmc$	$P6_3/mmc$
Z	4	4
a (Å)	5.228(1)	5.241(1)
c (Å)	8.5320(1)	8.492(1)
Volume (Å^3)	201.95(6)	202.01(6)
$d_{calcd.}$ (g/cm^3)	5.206	5.246
Reflections/R_{int}	1161/ 0.0216	1101/ 0.0428
Data/restr./para.	115/0/12	116/0/11
GOF on F^2	1.167	1.280
R_1/wR_2 [$I>2\sigma(I)$]	0.0165/0.0351	0.0428/0.1000
(all data)	0.0184/0.0362	0.0457/0.1023
Residues (e/Å^3)	0.529/–0.856	1.807/–1.217

As the content of Sc increases from crystals $Mg_{0.84(1)}Sc_{0.16(1)}Zn_2$ to $Mg_{0.78(1)}Sc_{0.22(1)}Zn_2$, the Sc/Mg–Zn1 distances are shortened by approximately 0.03 Å, but the Sc/Mg–Zn2 distances are enlarged by approximately 0.01–0.03 Å. The anisotropic effects incurred by Sc/Mg alloying also lead to longer Zn2–Zn2 bond distances in the Kagomé nets, in the *ab* plane, and shorter Zn1–Zn2 interlayer bonds (Table 3). As a result, the lattice parameter a is expanded but c is squeezed with increasing y, as observed in experiments (Figure 1). However, such changes cannot pervade in the whole composition range (between $MgZn_2$ and $ScZn_2$), because too large Zn2–Zn2 and too short Zn1–Zn2 distances will result in severe geometry distortion that will finally lead the structure to collapse or, from the viewpoint of energy, it will build up so much internal stress that will drive the structure into "explosion".

Table 3. Comparison of important bond lengths (Å) in $Mg_{0.84(1)}Sc_{0.16(1)}Zn_2$ and $Mg_{0.78(1)}Sc_{0.22(1)}Zn_2$.

Bonds	$Mg_{0.84(1)}Sc_{0.16(1)}Zn_2$	$Mg_{0.78(1)}Sc_{0.22(1)}Zn_2$
Zn1–Zn2	2.6299(4)	2.6258(7)
Zn2–Zn2	2.563(1)	2.565(2)
Zn2–Zn2	2.665(1)	2.676(2)
Sc–Zn1	3.0646(7)	3.033(4)
Sc–Zn2	3.047(2)	3.070(2)
Sc–Zn2	3.066(1)	3.0710(9)

Bonding

To further explain the above experimental observations, electronic structure calculations and bonding analyses were employed for hypothetical $Mg_{0.5}Sc_{0.5}Zn_2$ models in which Sc and Mg are alternatively ordered, as LMTO-ASA calculations cannot handle structural models with disordered atoms. Three models with the same unit cells are possible; they have space group $P\bar{3}m1$, $P6_3mc$, and $P\bar{6}m2$. According to the calculations, however, the last model with $P\bar{6}m2$ symmetry gave the lowest total energy. Therefore, this model was used for the following discussion.

Figure 3 shows the density-of-states (DOS) and the crystal overlap Hamilton population (COHP) data for Zn1–Zn2

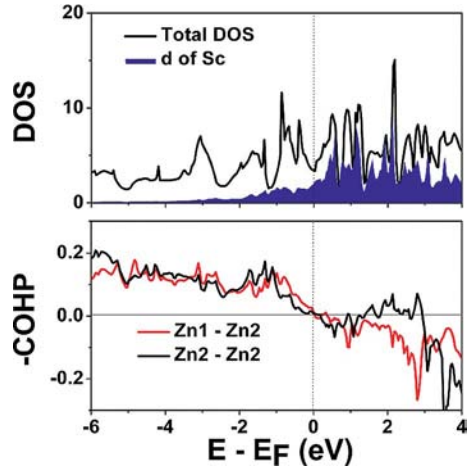

Figure 3. The density-of-states (DOS, states/ev/cell) and crystal overlap Hamilton population (COHP, eV bond^{-1} mol^{-1}) for the hypothetical $Mg_{0.5}Sc_{0.5}Zn_2$ ($P\bar{6}m2$), in which Sc and Mg atoms are ordered.

and Zn2–Zn2 homoatomic covalent bonds in the anionic framework for the hypothetical $Mg_{0.5}Sc_{0.5}Zn_2$ ($P\bar{6}m2$) model. Judging from the total DOS, the Fermi energy is located in a prominent pseudogap of a continuous DOS pattern, characteristic of polar intermetallics with strong covalent bonding. As in $MgZn_2$,[31] the Sc 4s, 4p states, Mg 2s, 2p states, and Zn 3p, 4s states span the entire energy range, suggesting that they mix throughout the whole valence band. The Zn 3d states are core-like states far below the Fermi energy (not shown), without significant interaction with other states. On the contrary, a considerable amount of Sc 3d states are located below the Fermi energy (shaded), which provides evidence of interaction with other states.

The Fermi energy clearly splits the bonding and antibonding states of both Zn1–Zn2 and Zn2–Zn2, the major bonds among the anionic network (above). This suggests that the hypothetical $Mg_{0.5}Sc_{0.5}Zn_2$ model is optimized in terms of structure, bonding, and composition. The last is consistent with the maximum solid solution of $Mg_{0.42–0.50}Sc_{0.58–0.50}Zn_2$ estimated from our experiments (above). By rigid band assumptions, excessive Sc (which has one more electron than Mg) would push the Fermi level in Figure 3 to an energetically unfavorable position with higher DOS and antibonding states. The last are actually observed in the DOS and COHP of the $ScZn_2$ Laves phase with extrapolated lattice parameters (above, see Figure S2). On the contrary, no such Zn–Zn antibonding state was observed for the $ScZn_2$ high-pressure phase, although the Fermi level remains at a high DOS (Figure S3). It appears that the major reason driving the $ScZn_2$ Laves phase to instability at ambient pressure is the unoptimized antibonding states in the Zn–Zn network. These states would lead to an enormous internal stress in the structure, which can be counterbalanced by optimized structure and bonding at high pressure.

In terms of the bonding characters of Sc–Zn and Mg–Zn in $Mg_{0.5}Sc_{0.5}Zn_2$, ionic character should be the dominant property, because of the apparent electron transfer from Sc/Mg to Zn, as expected; but the electron transfer is not complete, some electrons are still shared with Zn and form covalent bonds. Generally, the electron localization function (ELF) has been proven as a powerful tool to visualize covalent bonds, of which the paired electrons are expressed by bond attractors in space.[32–34] In this case, 2e–2c covalent bonding attractors on the Mg–Zn bonds and multicenter bonding attractors between Sc and Zn are evidently observed (Figure 4). The last appears to be new relative to those of CsK_2, $TiZn_2$, $MgZn_2$, $MgCu_2$, $TiBe_2$, and KPb_2 Laves phases,[25] which are apparently comprehensively influenced by factors such as size, packing, VEC, electronegativity, but not by any single one alone.

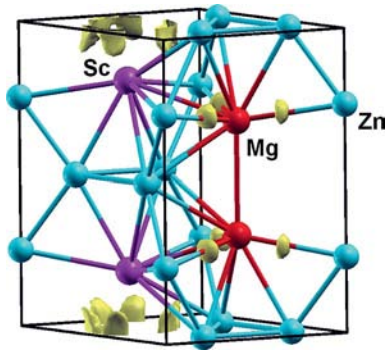

Figure 4. Electron localization function (ELF) for the Sc/Mg ordered model, $Mg_{0.5}Sc_{0.5}Zn_2$ ($P\bar{6}m2$). Covalent bonding attractors between the electropositive Sc/Mg atoms and the electronegative Zn atoms are shown at a cutoff isosurface of ELF = 0.48 (the maximum ELF is 0.505).

Conclusions

In this work, the alloy behavior between $MgZn_2$ and $ScZn_2$ Laves phases were investigated. Although both end members are isostructural, they were found to form a solid solution within a limited range, that is, $Mg_{1-y}Sc_yZn_2$ ($y <$ ca. 0.5). Single-crystal X-ray structural analyses revealed that the Zn2–Zn2 bonds in the *ab* plane and the Zn1–Zn2 interlayer bonds have different responses to the Sc/Mg alloy, resulting in strong geometric distortion that could lead to a structural explosion. Electronic structural analyses revealed that the $ScZn_2$ Laves phase at normal pressure is unfavorable in terms of structure and bonding.

Experimental Section

Synthesis: The starting materials were high-purity metals as received: Mg turnings, Zn particles, and Sc trunks (all >99.99%, Alfa-Aesar). Appropriate amounts of the metals (ca. 400 mg in total) were weighed in a N_2-filled glove box ($H_2O < 0.1$ ppm vol.) according to the formula $Mg_{1-x}Sc_xZn_2$ (x = 0.25, 0.33, 0.5, 0.67, and 0.75). The mixtures were weld-sealed under Ar into Ta containers, which were then enclosed in evacuated SiO_2 jackets ($< 10^{-5}$ Torr). All reactions were carried out under the same conditions: Samples were heated at 700 °C for 48 h, cooled to 400 °C at rate of 5 °C/h, annealed at that temperatue for 120 h, then air-quenched to room temperature. All products are brittle, inert to moisture, and shiny with metallic luster. Single crystals were picked from the respective crushed samples, and the remaining parts were ground into powder samples for phase analyses.

X-ray Diffraction

Phase analyses were made on the powder X-ray diffraction data obtained with the help of a Huber G670 camera equipped with monochromatic $K_{\alpha 1}$ radiation (λ = 1.540598 Å). Lattice parameters were refined by using 2θ values of the strong peaks within the range 20–70° with program Unitcell.[35] Single-crystal structure determinations were carried out with the aid of a Bruker APEX CCD single-crystal diffractometer equipped with graphite-monochromatized Mo-K_α (λ = 0.71069 Å) radiation. Intensity data were collected at room temperature at an ω scan mode with exposures of 10 s/frame. A total of 1315 frames were collected for each data set. Data integration, Lorentz polarization, empirical absorption, and other corrections were made by the SAINT and SADABS subprograms that are included in the SMART software package.[36] Full-matrix least-squares refinements on F_o^2 were performed with the aid of the SHELXTL v 6.1 program.[37]

The structures were determined by direct methods, from which all three independent positions were easily located. The assignment of Sc/Mg mixtures were judged according to respective isotropic displacement parameters. Independent refinements on respective site-occupancy parameters were also performed with isotropic displacement parameters, but all suggested full occupancies with standard deviations within 1σ. So, in the final refinements with anisotropic displacement parameters, the occupancy for each site was fixed to unity. The refined positional parameters standardized by TIDY[38] are listed in Table 1, together with isotropic displacement parameters. The data collections, refinement parameters, and crystallographic data are summarized in Table 2. The important interatomic distances calculated are listed in Table 3. Further details on the crystal structure investigations may be obtained from the Fachinformationszentrum Karlsruhe, 76344 Eggenstein-Leopoldshafen, Germany (fax: +49-7247-808-666; e-mail: crysdata@fiz-karlsruhe.de) on quoting the depository numbers CSD-422995 for $Mg_{0.78}Sc_{0.22}Zn_2$ and CSD-422996 for $Mg_{0.84}Sc_{0.16}Zn_2$.

Electronic Structure Calculations: The calculations were performed by means of the self-consistent, tight-binding, linear-muffin-tin-orbital (LMTO) method in the local density and atomic sphere approximations (LDA and ASA), within the framework of the DFT method.[39–42] The ASA radii for Mg, Zn, and Sc were automatically scaled with a maximal overlap restriction of 16%, and no interstitial spheres were introduced. Reciprocal space integrations were carried out by using the tetrahedron method. The basis sets used for calculations were: Mg 3s/3p/(3d), Zn 4s/4p/4d, and Sc 4s/(4p)/3d (down-folded orbitals shown in parentheses). The crystal overlap Hamilton population (COHP)[43] analyses were performed to gain insight into the bonding properties.

Supporting Information (see footnote on the first page of this article): Refined lattice parameters for selected compositions $Mg_{1-x}Sc_xZn_2$ ($x <$ ca. 0.25–0.75), experimental powder X-ray diffraction patterns, and DOS and COHP data for the $ScZn_2$ Laves phase at ambient pressure and high pressure.

Acknowledgments

This work is supported by the start-up research fund of the "Hundred Talent Program" Professorship of the University of Science and Technology of China and the Research Fund for the Doctoral Program of Higher Education of China (20103402110033).

[1] J. D. Corbett, *Inorg. Chem.* **2010**, *49*, 13.
[2] U. Häussermann, S. Amerioun, L. Eriksson, C.-S. Lee, G. J. Miller, *J. Am. Chem. Soc.* **2001**, *124*, 4371.
[3] Q. Lin, J. D. Corbett, *Inorg. Chem.* **2009**, *48*, 5403.
[4] D. C. Fredrickson, S. Lee, R. Hoffmann, *Angew. Chem. Int. Ed.* **2007**, *46*, 1958.
[5] M. L. Fornasini, P. Manfrinetti, D. Mazzone, S. K. Dhar, *Z. Naturforsch., Teil B* **2008**, *63*, 237.
[6] S. M. Kauzlarich, Chemistry, Structure, and Bonding of Zintl Phases and Ions, VCH, New York, **1996**.
[7] O. Gourdon, D. Gout, G. J. Miller, in *Encyclopedia of Condensed Matter Physics* (Eds.: B. S. Bassani, G. Liedl, P. Wyder), Elsevier, Amsterdam, Boston, **2005**, p. 409.
[8] G. J. Miller, C.-S. Lee, W. Choe, in *Inorganic Chemistry Highlights* (Eds.: G. Meyer, D. Naumann, L. Wesemann), Wiley-VCH, Weinheim, **2002**, p. 21.
[9] H. G. von Schnering, *Nova Acta Leopold.* **1985**, *59*, 165.
[10] H. Schäfer, W. Eisenmann, W. Müller, *Angew. Chem. Int. Ed. Engl.* **1973**, *12*, 694.
[11] K. Wade, *Adv. Inorg. Chem. Radiochem.* **1976**, *18*, 1.
[12] U. Mizutani in *The Science of Complex Alloy Phases* (Eds.: T. B. Massalski, P. E. A. Turchi), TMS (The Minerals, Metals & Materials Society), Warrendale, Pennsylvania, **2005**, p. 1.
[13] W. Hume-Rothery, *J. Inst. Met.* **1926**, *35*, 295.
[14] A. L. Johnston, R. Hoffmann, *Z. Anorg. Allg. Chem.* **1992**, *616*, 105.
[15] F. Laves, H. Witte, *Metallwirtschaft* **1936**, *15*, 15.
[16] J. B. Friauf, *Phys. Rev.* **1927**, *29*, 34.
[17] F. Laves, H. Witte, *Metallwirtschaft* **1935**, *14*, 645.
[18] F. C. Frank, J. S. Kasper, *Acta Crystallogr.* **1958**, *11*, 184.
[19] D. P. Shoemaker, C. B. Shoemaker, in *Introduction to Quasicrystals* (Ed.: M. V. Jarić), Academic Press, Inc., **1988**, p. 1.
[20] F. Laves, *Naturwissenschaften Z.* **1939**, *27*, 65.
[21] E. Zintl, A. Harder, *Z. Phys. Chem. Abt. B* **1932**, *16*, 206.
[22] G. E. R. Schulze, *Z. Elektrochem.* **1939**, *45*, 849.
[23] Y. Ohta, D. G. Pettifor, *J. Phys. Condens. Matter* **1990**, *2*, 8189.
[24] F. Stein, M. Palm, G. Sauthoff, *Intermetallics* **2004**, *12*, 713.
[25] A. Ormeci, A. Simon, Y. Grin, *Angew. Chem. Int. Ed.* **2010**, *49*, 8997.
[26] Q. Lin, J. D. Corbett, *Philos. Mag.* **2006**, *86*, 607.
[27] X. Liu, F. Rau, J. Breu, K. J. Range, *J. Alloys Compd.* **1996**, *243*, L5.
[28] A. Palenzona, P. Manfrinetti, *J. Alloys Compd.* **1997**, *247*, 195.
[29] T. Ohba, Y. Kitano, Y. Komura, *Acta Crystallogr., Sect. C* **1984**, *40*, 1.
[30] L. Pauling, *The Nature of the Chemical Bond*, 3rd ed., Cornell University Press, Ithaca, **1960**.
[31] M.-M. Wu, L. Wen, B.-Y. Tang, L.-M. Peng, W.-J. Dinf, *J. Alloys Compd.* **2010**, *506*, 412.
[32] U. Haüssermann, S. Wengert, P. Hoffmann, A. Savin, O. Jepsen, R. Nesper, *Angew. Chem. Int. Ed. Engl.* **1994**, *33*, 2069.
[33] A. Savin, R. Nesper, S. Wengert, T. F. Fässler, *Angew. Chem. Int. Ed. Engl.* **1997**, *36*, 1808.
[34] T. F. Fässler, *Chem. Soc. Rev.* **2003**, *32*, 80.
[35] T. J. B. Holland, S. A. T. Redfer, *Mineral. Mag.* **1997**, *61*, 65.
[36] *SMART*, Madison, WI, **1996**.
[37] *SHELXTL*, Madison, WI, **2000**.
[38] L. M. Gelato, E. Parthé, *J. Appl. Crystallogr.* **1987**, *20*, 139.
[39] R. Tank, O. Jepsen, A. Burkhardt, O. K. Andersen, Max-Planck-Institut für Festkörperforschung, Stuttgart, Germany, **1994**.
[40] H. L. Shriver, *The LMTO Method*, Springer-Verlag, Berlin, **1984**.
[41] O. Jepsen, M. Snob, "Linearized Band Structure Methods" in *Electronic Band Structure and Its Applications*, Springer Lecture Notes, Springer-Verlag, Berlin, **1987**.
[42] O. K. Anderson, O. Jepsen, *Phys. Rev. Lett.* **1984**, *53*, 2571.
[43] R. Dronskowski, P. Blöch, *J. Phys. Chem.* **1993**, *97*, 8617.

Received: March 28, 2011
Published Online: June 22, 2011

